Synthesis of Clay-Dispersed Poly(styrene-*co*-methyl methacrylate) Nanocomposite via Miniemulsion Atom Transfer Radical Polymerization: A Reverse Approach

Khezrollah Khezri,[1] Vahid Haddadi-Asl,[2] Hossein Roghani-Mamaqani,[2] Mehdi Salami-Kalajahi[2]

[1]*Department of Chemistry, Amirkabir University of Technology, Tehran, Iran*
[2]*Department of Polymer Engineering and Color Technology, Amirkabir University of Technology, Tehran, Iran*

Received 10 May 2011; accepted 17 July 2011
DOI 10.1002/app.35279
Published online 26 October 2011 in Wiley Online Library (wileyonlinelibrary.com).

ABSTRACT: Poly(styrene-*co*-methyl methacrylate) nanocomposites were synthesized using reverse atom transfer radical polymerization (RATRP) in miniemulsion. Cetyltrimethylammonium bromide (CTAB) as a cationic surfactant applicable at higher temperatures was used for miniemulsion stabilization. Successful RATRP was carried out by using 4,4′-dinonyl-2,2′-bipyridine (dNbPy) as ligand. Monodispersed droplets and particles with sizes in the range of 200 nm were revealed by dynamic light scattering (DLS). Conversion and molecular weight study was carried out using gravimetry and size exclusion chromatography (SEC) respectively. By adding clay content, a decrease in the conversion and molecular weight and an increase in the PDI value of the nanocomposites are observed. Thermal stability of the nanocomposites in comparison with the neat copolymer is revealed by thermogravimetric analysis (TGA). Increased T_g values by adding clay content was also obtained using differential scanning calorimetry (DSC). Scanning electron microscopy (SEM) images of the nanoconposite with 1 wt % of nanoclay loading, display monodispersed spherical particles with sizes in the range of $\sim$ 200 nm. SEM findings are more compiled with dynamic light scattering (DLS) results. Well-dispersed exfoliated clay layers in the polymer matrix of the nanocomposite with 1 wt % nanoclay loading is confirmed by transmission electron microscopy (TEM) images and X-ray diffraction (XRD) data. © 2011 Wiley Periodicals, Inc. J Appl Polym Sci 124: 2278–2286, 2012

Key words: poly(styrene-*co*-methyl methacrylate); exfoliated nanocomposite; miniemulsion; RATRP

INTRODUCTION

In the recent few years, polymer layered silicate nanocomposites attracted great attention as an advanced polymer material which is mainly because of enhancement of nanocomposites properties in comparison with the neat polymer.[1–4] Mechanical,[5] magnetic and electric properties,[6] thermal stability and flame retardancy,[7] gas permeation,[8] and modulus[9] of a polymer matrix can be improved by adding a small amount of nanoclay. Such improvement in overall properties of nanocomposites is achieved because of high aspect ratio and high strength of these inorganic nanoparticles. The traditional application of these nanocomposites has been the reinforcement of plastics by the addition of inorganic nanofillers. Hybrid nanocomposites provide an attractive and versatile platform for emerging high-added-value applications such as photovoltaic cells and light-emitting devices, lithium-ion batteries, supercapacitors, and biosensors.[10]

Depending on the level of clay platelets delamination and dispersion in a polymer matrix, nanocomposites are mainly phase separated, intercalated, or exfoliated structures.[11] In intercalated structure, single polymer chains penetrate into some of the galleries of layered silicate and therefore results in formation of alternating layers of polymer and inorganic layers.[3,4] In an exfoliated structure, silicate layers are completely delaminated and separated randomly in the polymer matrix. One of the most important routs of nanocomposite preparation is *in situ* polymerization method. In this method, monomer is used directly for swelling layered silicates and then polymer chains propagate in between the intercalated sheets. Polymerization can initiate by heat, radiation or diffusion of suitable initiator moieties into the galleries of swollen silicate layers.[4,11] *In situ* polymerization almost resulted in exfoliated morphology and therefore this technique is more interested.[12,13]

Controlled/living radical polymerization (CRP) provides simple and robust routes to synthesize well-defined and low polydispersity index polymers.[14] In this context, nitroxide-mediated polymerization (NMP),[15] reversible addition fragmentation chain transfer (RAFT),[16] and atom transfer radical polymerization (ATRP)[17] have extensively been studied. Some advantages of ATRP over the other CRP methods consist of its applicability to a wide

Correspondence to: V. Haddadi-Asl (haddadi@aut.ac.ir).

variety of monomers and polymerization systems, its less sensitivity to impurities, and commercial availability of its reactants.[18,19] Application of various initiation systems is another advantage of ATRP over the other CRP systems. Reverse atom transfer radical polymerization (RATRP) is a suitable method for circumventing oxidation problems of normal atom transfer radical polymerization. The reactants of this technique are less sensitive to oxygen and therefore it can easily be handled.[18]

Miniemulsion polymerization is a powerful technique for encapsulating inorganic materials such as pigments and clay platelets. In this system, micellar nucleation is avoided since the amount of surfactant is below the critical micelle concentration.[19] But, only hydrophobic ligands which can form complex with transitional metal and are soluble in polymerization loci (organic phase) are useful in this system.[20] Brij98 is a common nonionic surfactant in aqueous dispersed media,[21,22] but it can not stabilize miniemulsions at higher temperatures. However, CTAB as a cationic surfactant can stabilize miniemulsion systems at higher temperatures.[23] In miniemulsion, no ingredients need to be transported through the aqueous phase during the polymerization.[20]

A review of related literature indicates that free radical polymerization has been employed for synthesizing nanocomposites in aqueous dispersed media[24,25] and particularly miniemulsion systems frequently.[26,27] However, polymer nanocomposites with narrow molecular weight distribution can be prepared by using living radical polymerization such as nitroxide-mediated polymerization (NMP),[28] RAFT polymerization,[29] and ATRP.[30] Tong et al. synthesized polystyrene encapsulated saponite composite lattices via miniemulsion polymerization. According to their results, using saponite with average particle size of 50 nm, which is modified by a monomer reactive cationic surfactant results in high saponite-loaded polystyrene lattices (up to 30 wt %). The majority of the final lattices are spherical particles with sizes less than 100 nm.[26] Tong et al. studied kinetics of miniemulsion polymerization of styrene in the presence of organoclay. They found that in the presence of nanoclay, molecular weight of polystyrene decreases which is attributed to a decrease in diffusion rate of monomer and living polymer chains inside the monomer droplets.[31] Akat et al. synthesized poly(methyl methacrylate) and polystyrene nanocomposites via *in situ* free radical polymerization by using intercalated chain transfer agent modified clay layers. Their results exhibit enhancement of thermal stability of nanocomposites in comparison with the neat polymers.[32] Zhang et al. prepared PS/PMMA mixed polymer brushes on the surface of clay layers by using *in situ* free radical polymerization. They found that significant exfoliated structure can be achieved using *in situ* polymerization.[33] Bottcher et al. synthesized exfoliated PMMA nanocomposite via ATRP. They demonstrated that living/controlled graft polymerization from initiator modified silicate can be employed to synthesize nanocomposites.[30]

Samakande et al. have successfully synthesized two kinds of encapsulated polystyrene nanocomposites by RAFT mediated miniemulsion polymerization. In their report, nanocomposites were partially exfoliated at low clay content. Also, by adding clay content the morphology of nanocomposites turned into the intercalated structure.[34] Wang et al. synthesized clay-dispersed ABA triblock copolymer nanocomposite via normal ATRP.[35] Additionally, Simms et al. synthesized butyl methacrylate (BMA) by reverse ATRP in miniemulsion. They showed that Brij98 as a nonionic surfactant can not stabilized the miniemulsion; however, cetyltrimethylammonium bromide (CTAB) is capable of effectively stabilizing the miniemulsion system.[23]

In this work, RATRP was employed to synthesize exfoliated poly(styrene-*co*-methyl methacrylate) nanocomposites via *in situ* polymerization in miniemulsion. Reverse initiation technique was used for its less sensitivity to oxygen. Additionally, appropriate selection of hydrophobic ligand and also a surfactant which is stable at higher temperatures is considered to conduct a successful miniemulsion ATRP.

EXPERIMENTAL

Materials

Styrene (Aldrich, 99%) and methyl methacrylate (Merck, 99%) were passed through an alumina-filled column to remove inhibitors. Cloisite 30B, montemorillonite that goes through an ion-exchanged reaction with a surfactant methyl tallow-bis-2-hydroxyethyl quaternary ammonium (Southern Clay Products, Gonzales, TX) was stored in vacuum oven (60°C, 40 mmHg) before use. Copper (II) bromide ($CuBr_2$, Fluka, 99%), 4,4′-dinonyl-2,2′-bipyridine (dNbPy, Aldrich, 97%), hexadecane (HD, Aldrich, 99%), tetrahydrofuran (THF, Merck, 99%), 2,2′-azobisisobutyronitrile (AIBN, Acros), cetyltrimethylammonium bromide (CTAB, Merck, 97%), and neutral aluminum oxide (Aldrich, 99%) were used as received.

Synthesis of poly(styrene-*co*-methyl methacrylate) and its nanocomposites

Reverse atom transfer radical copolymerizations were performed in a 250-mL three-necked lab reactor which equipped with a reflux condenser, nitrogen inlet valve, and a magnetic stir bar that was placed in an oil bath thermostated at desired

temperature. A typical batch of copolymerization was run at 90°C in miniemulsion system with the molar ratio of 400 : 1 : 1 : 2 for [M] : [$CuBr_2$] : [AIBN] : [dNbPy] giving a theoretical polymer molecular weight of 40,804 g mol^{-1} at 100% conversion. An organic phase was prepared by the addition of $CuBr_2$ (0.039 g, 0.174 mmol), dNbPy (0.142 g, 0.349 mmol), Hexadecane (0.37 mL, 1.28 mmol), and styrene (4 mL, 34.9 mmol) to a beaker and stirring over night at room temperature to form a homogeneous green solution. Also, a desired amount of nanoclay (0.5, 1, and 2 wt % versus monomer) were added to styrene (1.33 mL, 11.6 mmol) and methyl methacrylate (2.47 mL, 23.2 mmol) in another beaker and stirring was continued at room temperature over night to form homogeneous solution. The organic phase was prepared by mixing of two homogeneous solutions. The aqueous phase which consists of surfactant (CTAB, 0.3 g, 17 m*M*) and deionized water (48 mL) was stirred for another 1 h to form clear solution. AIBN as a radical initiator which is soluble in organic phase was added to the organic solution before mixing of aqueous and organic phases (0.028 g, 0.174 mmol). Then, the aqueous surfactant solution was added to the organic phase and the solution was stirred about 15 min before sonicating. Subsequently, the miniemulsion solution was immediately transferred into the reactor which was purged with nitrogen three times and then the reactor temperature was increased to 90°C. In the beginning of the reaction, polymerization media was light green and gradually changed to light brown. Samples were taken at the end of the reaction to measure the monomer conversion and particle size distribution. In designation of the samples, PSMM implies the neat poly(styrene-*co*-methyl methacrylate) and PSMNM*X* address the poly(styrene-*co*-methyl methacrylate) nanocomposites where "*X*" presents clay percentage (wt %) in the polymer matrix. For the all the samples, time of monomer and clay dispersion prior to the polymerization was 15 h.

Separation of polymer chains from clay platelets and catalyst removal

For separating polymer chains from clay platelets, nanocomposites were dissolved in THF. By high-speed ultracentrifugation and then passing the solution through a 0.2-μm filter, polymer chains were separated from clay platelets. Subsequently, polymer solutions passed through an alumina column to remove catalyst.

Characterization

Droplet and particle size distributions were measured by dynamic light scattering (DLS, Malvern nano zetasizer ZS 90, UK) with a scattering angle of 176.1. The reported diameters is an intensity-weighted average particle size (*z*-average), comprised of two measurements and the errors have been estimated to be 3% or less. Before the measurements, samples were diluted by surfactant aqueous solution to reduce the effect of dilution on the droplets and particles size. Emulsification process was performed by employing a probe ultrasound (Hielscher UIP1000hd, 20 kHz, Germany). Final monomer conversion was determined gravimetrically. Size exclusion Chromatography (SEC) was used to measure the molecular weight and molecular weight distribution. A Waters 2000 ALLIANCE with a set of three columns of pore sizes of 10,000, 1000, and 500 Å was utilized to determine polymer average molecular weight and polydispersity index (PDI). THF was used as the eluent at a flow rate of 1.0 mL min^{-1}, and calibration was carried out using low polydispersity polystyrene standards. X-ray diffraction spectra were collected on an X-ray diffraction instrument (Siemens D5000) with a Cu target ($\lambda = 0.1540$ nm) at room temperature. The system consists of a rotating anode generator operated at 35 kV and 20 mA current. The samples were scanned from $2\theta = 2^\circ$ to 10° at the step scan mode, and the diffraction pattern was recorded using a scintillation counter detector. The basal spacing or d_{001}-spacing of the samples were calculated using Bragg's equation ($\lambda = 2d\sin\theta$). Thermal analyses were carried out using a differential scanning calorimetry (DSC) instrument (NETZSCH DSC 200 F3, Netzsch, Selb/Bavaria, Germany). Nitrogen at a rate of 50 mL min^{-1} was used as the purging gas. Aluminum pans containing 2–3 mg of the samples were sealed using the DSC sample press. The samples were heated from ambient temperature to 190°C at a heating rate of 10°C min^{-1}. Thermal gravimetric analyses were carried out with a PL thermogravimetric analyzer (Polymer Laboratories, TGA 1000, UK). The thermograms were obtained from ambient temperature to 650°C at a heating rate of 10°C min^{-1}. A sample weight of about 7 mg was used as the purging gas at a flow rate of 50 mL min^{-1}; an empty pan was used for all the measurements, and nitrogen was used as the reference. A transfer electron microscope, Philips EM 208, with an accelerating voltage of 200 kV was used to study the morphology of the nanocomposites. Samples of 70 nm thickness were prepared by Reichert ultra microtome (type OMU 3). Surface morphology of powder samples was examined by Scanning Electron Microscope (SEM: Philips XL30) with acceleration voltage of 17 kV.

RESULTS AND DISCUSSION

Poly(styrene-*co*-methyl methacrylate) nanocomposites synthesized by reverse atom transfer radical polymerization. General procedure of copolymerization is

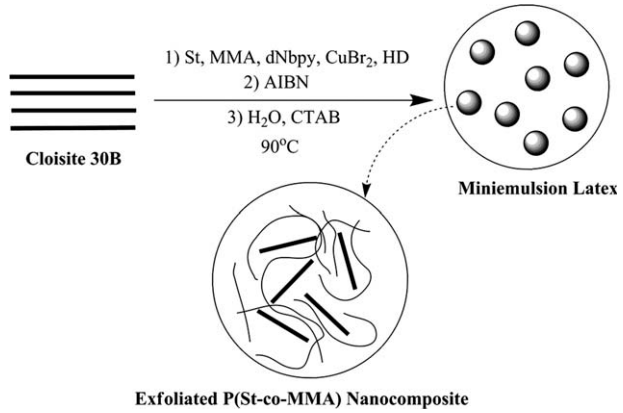

Scheme 1 General procedure for preparation of poly (styrene-*co*-methyl methacrylate) nanocomposites.

illustrated in Scheme 1. Although Brij98 is a common surfactant for aqueous dispersed ATRP, its application was restricted since it can not stabilize miniemulsion systems at higher temperatures. Therefore, CTAB as a cationic surfactant which is an effective surface active material at higher polymerization temperatures was employed.[23] Using dNbpy as a hydrophobic ligand causes metal complex to stay in the polymerization loci. Also, for nucleation of the majority of droplets, an oil-soluble initiator was employed. Additionally, to prevent the Ostwald ripening phenomena, hexadecane which is a low molecular weight hydrophobe was used as a cosurfactant. Therefore, using hexadecane and CTAB improves the stability of tiny monomer droplets and particles during polymerization at higher temperatures.[36,37]

DLS was employed to determine droplet and particle size distributions. Also, monodispersity of droplets and particles can be evaluated by this technique. Figures 1 and 2 display DLS curves for the droplets and particles respectively.

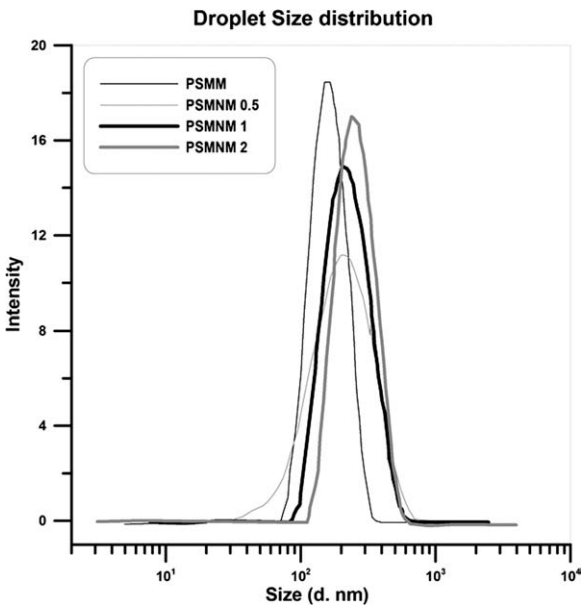

Figure 1 Droplet size distribution of the neat copolymer and its nanocomposites.

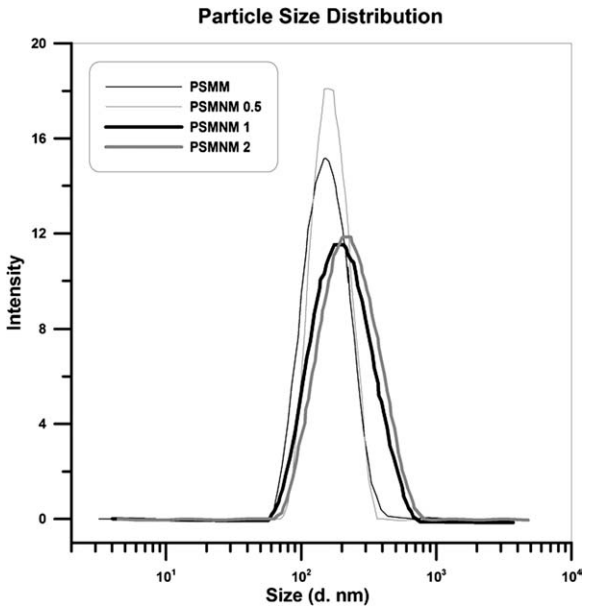

Figure 2 Droplet size distribution of the neat copolymer and its nanocomposites.

According to the results of DLS, there is no peak in the range of about 10 nm which indicates that there are no micelles in the reaction medium. The extracted data from the DLS curves which are summarized in Table I shows that droplet and particle sizes are in the range of miniemulsion particle and droplet sizes.[19] PDI values demonstrate monodisperse droplet and particle size distributions which more clarifies an efficient homogenization. Average particle size of the neat copolymer latex is smaller in comparison with its nanocomposites lattices and the average particle size increases by increasing clay content. These findings are evidences for clay platelets inference in the particles which indicates that the content of clay in the particles increases by increasing clay content in the polymer matrix (similar results observed for droplet size distribution).[27]

As shown in Figure 3, there is a shoulder in SEC traces of all the samples. Also, their polydispersity indexes are relatively high. According to the fact that block copolymer can not be synthesized by

TABLE I
Droplet and Particle Sizes and PDI Values

Sample designation	Droplet size (d. nm)	PDI	Particle size (d. nm)	PDI
PSMM	148	0.06	138	0.10
PSMNM 0.5	168	0.20	147	0.07
PSMNM 1	197	0.13	167	0.17
PSMNM 2	227	0.11	190	0.19

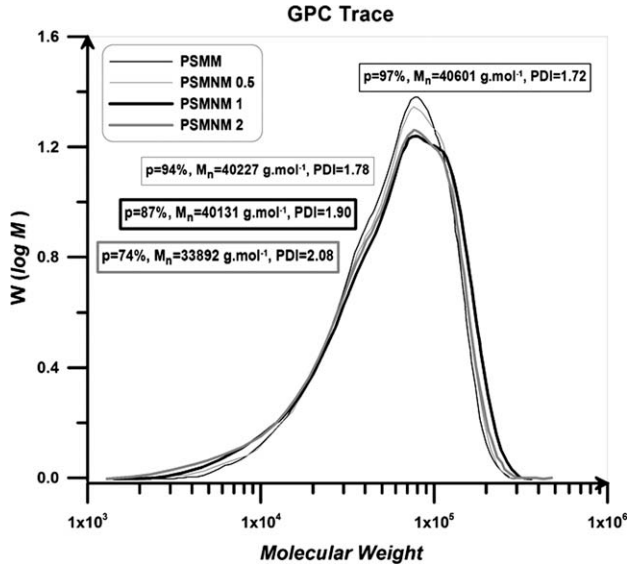

Figure 3 GPC traces of the neat copolymer and its nanocomposites.

reverse initiation technique, shoulders can not be attributed to the formation of a block copolymer.[18] According to the related literature, radical coupling can be resulted in such shoulders.[38] In the case that concentration of deactivator in the polymerization loci is not sufficiently high to reduce radical concentration; coupling of propagating radicals can be occurred and results in relatively high polydispersity index of nanocomposites. In addition, AIBN-induced living radical polymerization always results in polymers with high PDI value when the molar ratio of the deactivator to that of the initiating radicals is equal to unity. Only by higher amount of deactivator, lower values of PDI can be obtained.[39] Also, concentration of deactivator in organic phase is decreased at higher temperatures which is the result of the variation of deactivator partitioning behavior by varying temperature.[40]

Broadening of SEC curves by adding clay content indicates that nanoclay as a filler affects the equilibrium of ATRP reaction and leads to higher PDI values. According to the data presented in Table II, PDI values increases by adding nanoclay content. Nanoclay as an impurity can increase chain transfer and termination reaction of propagating radicals, and therefore broadens molecular weight distribution of the resultant polymers.[13,31] Table II shows that there is an appropriate agreement between the theoretical and experimental molecular weights which in combination with the system color change from light green to light brown in the beginning of the reaction clarified the living nature of copolymerization.[36,41] The decrease of monomer conversion and molecular weight of resultant polymers by increasing clay content indicates that clay platelets apply a confinement effect on the polymerization reaction. Penetration of monomer, initiator, and metal complex into the interlayer galleries of nanoclay can be retarded; therefore, probability of chain propagation and monomer consumption decreases by increasing the clay content.[31] In the presence of clay layers, irreversible reaction between the clay functionalities and growing radicals result in termination reactions.[34] Retarding effect of nanoclay on the polymerization rate was also reported in other works.[27,31]

The nanoclay used in this work belongs to the general family of 1 : 2 phillosilicates. Its crystal structure consists of platelets with an inner octahedral layer sandwiched between two silicate tetrahedral layers. The platelets thickness is around 1 nm and the lateral dimensions of these layers vary from 30 nm to several microns.[1,11] X-ray diffraction is a useful technique for examining the effect of polymer chains and clay surface interaction on the order of the clay platelets in the matrix. XRD diffractograms also provide beneficial information about *d*-spacing of the intercalated hybrids by following Bragg's law of diffraction at the peak positions.[3,42]

Figure 4 presents XRD patterns of cloisite 30B, neat copolymer, and prepared nanocomposites. All the nanocomposites synthesized using *in situ* polymerization reveal no noticeable peak which indicates that clay layers exfoliated in the copolymer matrix. Disappearance of diffraction peak in the nanocomposites is a result of shifting *d*-spacing value of (001) plane (d_{001}) to corresponding diffraction angles of smaller than 2°. This indicates that the gallery distance of clay layers increases by inserting copolymer chains. Therefore, the gallery distance of clay platelets increases as a resultant of the penetration of copolymer chains into them. However, in the case of the nanocomposite which is prepared by using solution blending technique, an obvious diffraction peak

TABLE II
MWs and PDI Values of Extracted Polymers

Sample	Reaction time (h)	Conversion (%)	M_n (g mol^{-1}) Exp.	M_n (g mol^{-1}) Theo.	M_w (g mol^{-1})	PDI
PSMM	22	97	40,601	39,580	70,053	1.72
PSMNM 0.5	22	94	40,227	38,356	71,785	1.78
PSMNM 1	22	87	40,131	35,500	76,341	1.90
PSMNM2	22	74	33,892	30,195	70,545	2.08

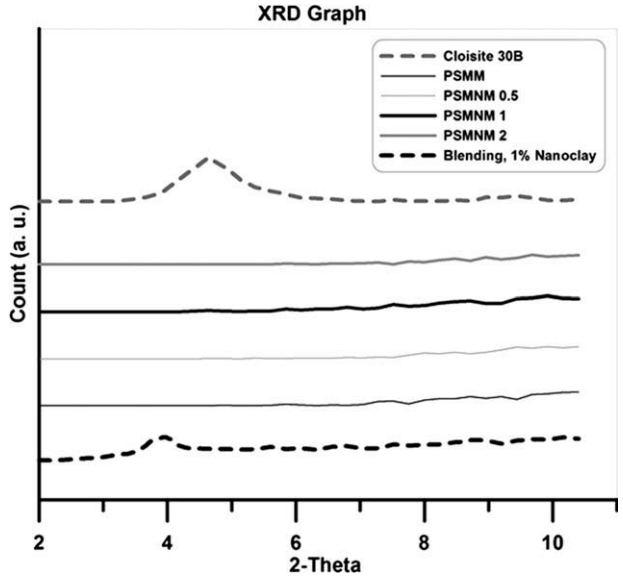

Figure 4 X-ray diffraction patterns of the neat copolymer and its nanocomposites.

is observed. In comparison with the neat cloisite 30B, its diffraction peak is shifted to smaller diffraction angle, which indicates that the gallery distance of clay layers increased by penetrating some of the copolymer chains into them and intercalated morphology is formed.

Thermogravimetric analysis (TGA) was used to study thermal stability of the neat copolymer and its nanocomposites. TGA thermograms of weigh loss as a function of temperature in the temperature window of 50–650°C in addition to their corresponding differential thermogravimetric curves (DTG) are presented in Figure 5.

According to the Figure 5, thermal stabilities of all the nanocomposites are higher than the neat copolymer. Also, degradation temperature of the nanocomposites rises by increasing the clay content. TGA data summarized in Table III shows the temperature threshold at which 10% of the copolymer and its nanocomposites degradation is takes place ($T_{0.1}$). In addition, char values of the samples at 600°C are presented. As it is expected, the percentage of char

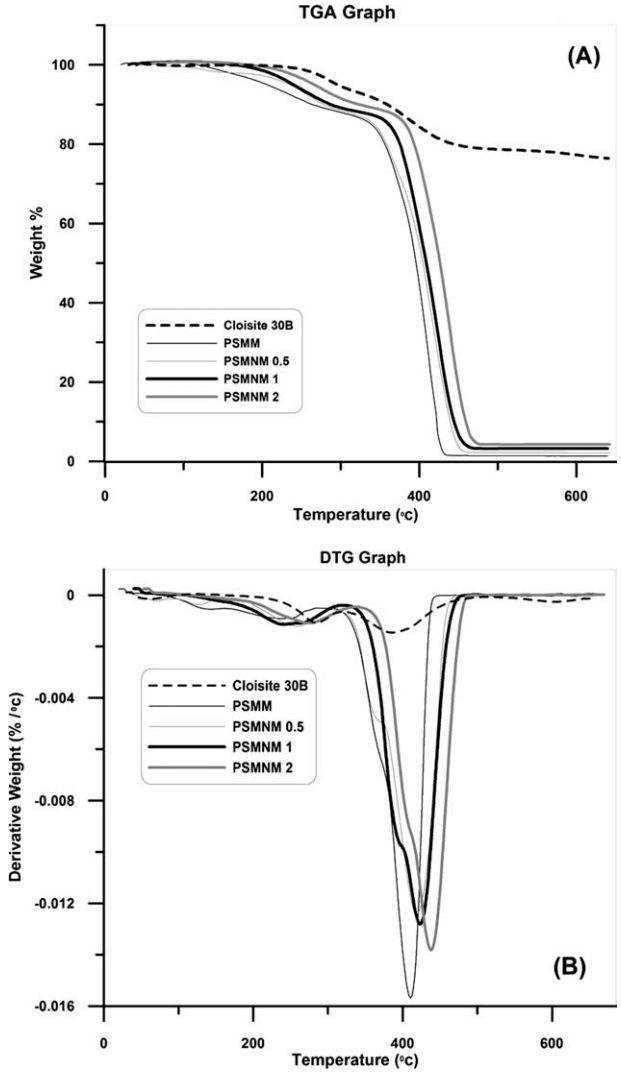

Figure 5 (A) TGA and (B) DTG thermograms of the neat copolymer and its nanocomposites.

values increases by increasing clay content. Also, cloisite 30B leaves 77.27% char after complete degradation at 600°C.

Increasing of degradation temperature of nanocomposites by adding nanoclay content is attributed to the high thermal stability of nanoclay and also

TABLE III
TGA, DTG, and Glass Transition Temperature Data of the Neat Copolymer and Its Nanocomposites

	TGA		DTG								DSC	
			Onset degradation (°C)			Mid-point degradation (°C)		Final degradation (°C)				
Sample designation	$T_{0.1}$ (°C)	Char (%)	Start	Peak	End	Start	End	Start	Peak	End	M_n (g mol^{-1})	T_g (°C)
PSMM	259	1.33	168	234	278	313	364	375	410	441	40,601	67
PSMNM 0.5	275	2.09	172	249	297	318	370	376	418	466	40,227	75.3
PSMNM 1	283	3.35	176	251	310	332	394	402	423	474	40,131	85.8
PSMNM 2	316	4.34	197	273	328	351	405	412	437	484	33,892	69.7
Cloisite 30B	356	77.27	–	–	–	–	–	–	–	–	–	–

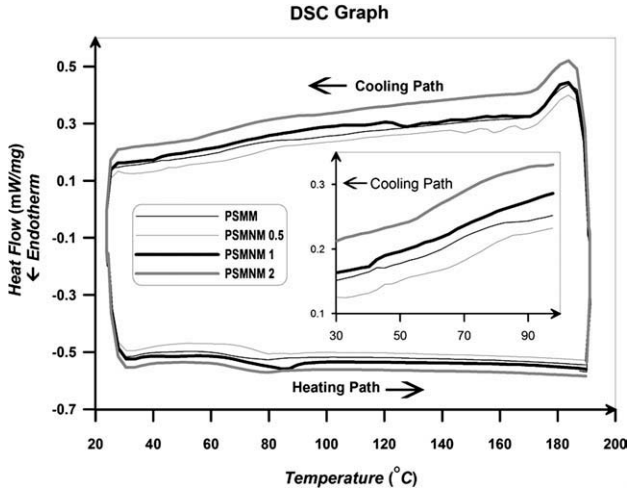

Figure 6 DSC Thermogram for the neat copolymer and its nanocomposites.

interaction between clay platelets and copolymer matrix.[43] Additionally, hindrance effect of nanoplatelets on the polymer chains movement and restriction of oxygen permeation by the silicate sheets are the other reasons for higher thermal stability of nanocomposites.[13,35] Except for the degradation of volatile materials (residual monomer and clay functionalities), three degradation steps are observed in the thermograms, which can be ascribed to the methyl methacrylate segments of the copolymer. In the case of methyl methacrylate, head-to-head linkages, chain unsaturation, and random scission can be achieved; therefore, its thermogram reveals three degradation steps.[32,44] Table III summarizes the extracted data from DTG curves which indicates an improvement in thermal stability of nanocomposites by increasing clay content.

Differential scanning calorimetry (DSC) was used to evaluate thermal behavior of the neat copolymer and its nanocomposites with different clay loadings and the results are displayed in Figure 6. Because clay platelets do not bear any transition in this range of temperature, therefore merely thermal transition of polymers is observed. In the DSC analysis, samples were heated from room temperature to 190°C. Then, they were cooled to room temperature for distinguishing the phase conversion and other irreversible thermal behaviors. And finally, samples were heated from room temperature to 190°C to evaluate T_g values.

In the heating path, an obvious inflection is appeared which shows glass transition temperature of the samples. Also, there is not any peak in the cooling path which indicates that the structure of synthesized copolymer and its nanocomposites are mainly amorphous and they have not gone through crystallization phenomenon. Extracted data from DSC graph (cooling path) is presented in Table III. According to these results, T_g values of nanocomposites with 0.5, 1, and 2 wt % of nanoclay loading are higher than the neat copolymer. Increasing T_g values by adding nanoclay content in the copolymer matrix can be attributed to the confinement effect of clay platelets.[13] The rigid two-dimensional clay platelets can restrict the steric mobility of polymer chains and causes the inflection in the DSC graphs starts at higher temperatures. Although it was expected that glass transition temperature of the nanocomposite with 2 wt % nanoclay loading (PSMNM 2) to be higher than the others, its T_g value does not follow this prediction due to its considerable low molecular weight. Therefore, its T_g is lower than PSMNM 1 and PSMNM 0.5, meanwhile it is higher in comparison with the neat copolymer. Copolymer nanocomposite

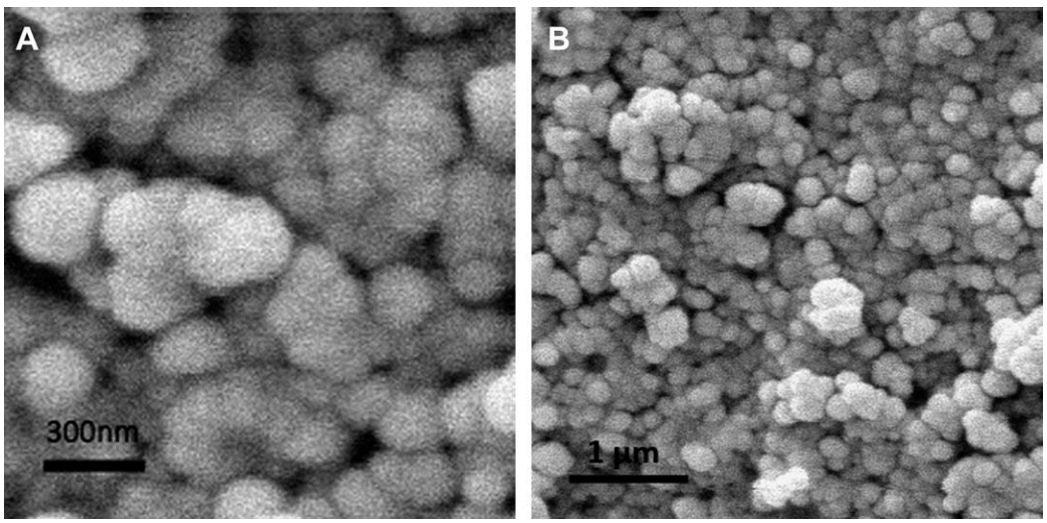

Figure 7 SEM image of PSMNM 1.

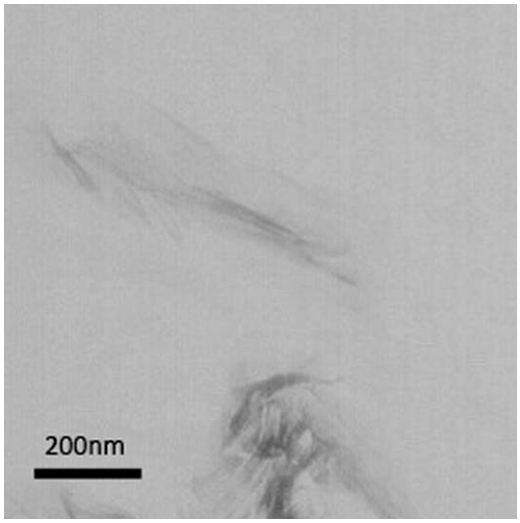

Figure 8 TEM image of PSMNM 1.

exhibits a single broad peak of higher intensity at below T_g. Significant increase in the intensity of this peak by adding clay content indicates that relaxations of the flexible copolymer segments decrease due to the increase of interfacial adhesion i.e., the highest interaction occurs between copolymer units and clay platelets.[45] It is also worth-mentioning that reactivity ratio of styrene and methyl methacrylate are approximately the same. Therefore, formation of a random copolymer is revealed and is more justified by a single T_g in the DSC thermogram.

Scanning electron microscopy (SEM) is a powerful technique for investigating the morphology of polymer nanocomposites. Figure 7 presents SEM micrographs of poly(styrene-*co*-methyl methacrylate) nanocomposite powder containing 1 wt % of cloisite 30B (PSMNM 1) in two different magnifications. Spherical shape of particles and monodispersity of particles size distribution in the range around 200 nm are extracted from these images which all in all express successful miniemulsion polymerization. These results are more coincide with the data extracted from DLS curves.

In addition to XRD characterization, transmission electron microscopy (TEM) as a useful analysis has been employed to investigate the clay platelets delamination and dispersion in the copolymer matrix. TEM micrograph of poly(styrene-*co*-methyl methacrylate) nanocomposite containing 1 wt % of cloisite 30B (PSMNM 1) is presented in Figure 8. In this image, the light and dark areas display poly (styrene-*co*-methyl methacrylate) matrix and silicate layers, respectively. As it is clear in the following image, silicate layers are disordered, dispersed, and well delaminated in the polymer matrix which indicates that an exfoliated morphology is formed. This result is more confirmed by the data extracted from XRD analysis.

CONCLUSIONS

Reverse atom transfer radical polymerization (RATRP) was employed to synthesize poly(styrene-*co*-methyl methacrylate) and its nanocomposites with different clay contents in miniemulsion. DLS results show that monodisperse droplets and particles with sizes in the range of around 200 nm are formed. SEC results reveal a monomodal peak with a shoulder. Additionally, by increasing clay content a decrease in the molecular weight of the nanocomposites was observed. However, polydispersity index of the extracted polymer chains are relatively high and increases by the addition of nanoclay content. XRD patterns display no considerable peak in diffraction angles of about $2\theta = 4$–6° which indicates that stacked silicate layers are completely exfoliated. Thermal stability of the nanocomposites is higher than the neat copolymer. Also, degradation temperature increment of all the three steps for nanocomposites was appeared using TGA and DTG data. SEM images display monodisperse distribution of spherical poly(styrene-*co*-methyl methacrylate) nanocomposite particles in PSMNM 1 which is more coincided with DLS analysis. Delaminated and dispersed clay platelets in the polymer matrix of PSMNM 1 are revealed by TEM analysis and the results is more complied with the results of XRD analysis. Therefore, completely exfoliated nanocomposites are synthesized by RATRP in miniemulsion system.

References

1. Ray, S. S.; Okamoto, M. Prog Polym Sci 2003, 28, 1539.
2. Fu, X.; Qutubuddin, S. Polymer 2001, 42, 807.
3. Zanetti, M.; Lomakin, S.; Camino, G. Macromol Mater Eng 2000, 279, 1.
4. Nguyen, Q.; Baird, D. Adv Polym Techn 2006, 25, 270.
5. Fujimori, A.; Ninomiya, N.; Masuko, T. Polym Adv Technol 2008, 19, 1735.
6. Caruso, F.; Spasova, M.; Susha, A.; Giersig, H.; Caruso, R. A. Chem Mater 2001, 13, 109.
7. Jang, B. N.; Costache, M.; Wilkie, C. A. Polymer 2005, 46, 10678.
8. Nazarenko, S.; Meneghetti, P.; Julmon, P.; Olson, B.; Qutubuddin, S. J Polym Sci B Polym Phys 2007, 45, 1733.
9. Shia, D.; Hui, C. Y.; Burnside, S. D.; Giannelis, E. P. Polym Composite 1998, 19, 608.
10. Tao, Y.; Endo, M.; Inagaki, M.; Kaneko, K. J Mater Chem 2011, 21, 313.
11. Alexandre, M.; Dubois, P. Mater Sci Eng 2000, 28, 1.
12. Roghani-Mamaqani, H.; Najafi, M.; Salami-Kalajahi, M.; Haddadi-Asl, V. Polym Composite 2010, 31, 1829.
13. Roghani-mamaqani, H.; Haddadi-Asl, V.; Najafi, M.; Salami-Kalajahi, M. AIChE J 2011, 57, 1873.
14. Cunningham, M. F. Prog Polym Sci 2002, 27, 1039.
15. Georges, M. K.; Veregin, R. P. N.; Kazmaier, P. M.; Hamer, G. K. Macromolecules 1993, 26, 2987.
16. Smulders, W.; Jones, C. W.; Schork, F. J. AIChE J 2005, 51, 1009.
17. Hatami, L.; Haddadi-Asl, V.; Roghani-Mamaqani, H.; Ahmadian-Alam, L.; Salami-Kalajahi, M. Polym Composite 2011, 32, 967.

18. Roghani-Mamaqani, H.; Najafi, M.; Salami-Kalajahi, M.; Haddadi-Asl, V. J Appl Polym Sci 2011, 120, 1431.
19. Qiu, J.; Charleux, B.; Matyjaszewski, K. Prog Polym Sci 2001, 26, 2083.
20. Min, K.; Matyjaszewski, K. Cent Eur J Chem 2009, 7, 657.
21. Eslami, H.; Zhu, S. Polymer 2005, 46, 5484.
22. Min, K.; Gao, H.; Matyjaszewski, K. J Am Chem Soc 2006, 128, 10521.
23. Simms, R. W.; Cunningham, M. F. J Polym Sci A Polym Chem 2006, 44, 1628.
24. Pan, M.; Shi, X.; Li, X.; Hu, H.; Zhang, L. J Appl Polym Sci 2004, 94, 277.
25. Kim, T. H.; Jang, L. W.; Lee, D. C.; Chio, H. J.; Jhon, M. S. Macromol Rapid Commun 2002, 23, 191.
26. Tong, Z.; Deng, Y. Polymer 2007, 48, 4337.
27. Tong, Z., Deng, Y. Ind Eng Chem Res 2006, 45, 2641.
28. Fujii, S.; Armes, S. P. Langmuir 2006, 22, 4923.
29. Salem, N.; Shipp, D. A. Polymer 2005, 46, 8573.
30. Roghani-Mamaqani, H.; Najafi, M.; Salami-Kalajahi, M.; Haddadi-Asl, V. J Appl Polym Sci, DOI: 10.1002/app.34511.
31. Tong, Z, Deng, Y. Macromol Mater Eng 2008, 293, 529.
32. Akat, H.; Tasdelen, M. A.; Prez, F. D.; Yagci, Y. Eur Polym J 2008, 44, 1949.
33. Zhang, J.; Yang, Y.; Zhao, C.; Zhao, H. J Polym Sci A Polym Chem 2007, 45, 5329.
34. Samakande, A.; Sanderson, R.; Hartmann, P. J Polym Sci A Polym Chem 2008, 46, 7114.
35. Wang, Y.-P.; Pei, X.-W.; Liu, X.-J.; Yuan, K.; Zhang, D.-X.; Li, Q.-L.; Wang, Y.-F. Polym Composite 2005, 26, 465.
36. Matyjaszewski, K.; Qiu, J.; Tsarevsky, N.; Charleux, B. J Polym Sci A Polym Chem 2000, 38, 4724.
37. Zetterlund, P. B.; Kagawa, Y.; Okubo, M. Chem Rev 2008, 108, 3747.
38. Cheng, S.; Xu, Z.; Yuan, J.; Ji, P.; Xu, J.; Ye, M.; Shi, L. J Appl Polym Sci 2000, 77, 2882.
39. Najafi, M.; Roghani-Mamaqani, H.; Salami-Kalajahi, M.; Haddadi-Asl, V. Chin J Polym Sci 2010, 28, 483.
40. Huang, J.; Jia, S.; Siegwart, D. J.; Kowalewski, T.; Matyjaszewski, K. Macromol Chem Phys 2006, 207, 801.
41. Li, M.; Matyjaszewski, K. Macromolecules 2003, 36, 6028.
42. Yilmazer, U.; Ozden, G. Polym Composite 2006, 27, 249.
43. Subramania, S.; Choia, S. W.; Lee, J. Y.; Kim, J. H. Polymer 2007, 48, 16, 4691.
44. Costache, M. C.; Wang, D.; Heidecker, M. J.; Manias, E. Polym Adv Technol 2006, 17, 272.
45. Soylemez, E.; Caylak, N.; Rzayev, Z. M. O. Express Polym Lett 2008, 2, 639.